Performance and Stability of Solid Oxide Cell Stacks in CO_2 Electrolysis Mode

F. Thaler, Q. Fang, U. de Haart, L. G. J. de Haart, R. Peters, and L. Blum

Forschungszentrum Jülich GmbH, Institute of Energy and Climate Research (IEK), Wilhelm-Johnen-Straße, 52425 Jülich, Germany

Compared to low-temperature electrolysis techniques, solid oxide cell (SOC) technology has attracted growing interest in Power-to-X scenarios based on renewable energy due to its high efficiency, reversibility, and the possibility of simultaneously converting CO_2 and H_2O into syngas, a chemical precursor for synthetic fuels or intermediates such as methanol. Furthermore, SOCs can also be operated in CO_2 electrolysis mode in order to produce pure CO, which is in great demand in the chemical and steel industries. Based on previous experience with fuel cell, steam- and co-electrolysis operation, the electrochemical performance and durability of planar fuel electrode-supported SOC stacks are investigated with a focus on CO_2 electrolysis. Their current-voltage characteristics and electrochemical impedance have been measured in both CO_2 and co-electrolysis modes. The main aim of these investigations was to gain insights into the electrochemical processes and limitations of the currently used electrodes during CO_2 electrolysis, and to understand the general degradation mechanisms of cells under different conditions. Using state-of-the-art cells, the stack can be operated at 800 °C with a current density of -1000 mA cm^{-2} below cell voltages of 1.4 V in a CO_2/CO (1:1) mixture. Based on the findings thus far, some promising approaches with respect to the optimization of fuel electrode microstructures and reaction kinetics to increase the performance and durability of the cells under CO_2 electrolysis operation are discussed.

Introduction

The energy transition strategy in Europe, moving from reliance on nuclear and fossil fuel-fired power plants to renewable energy sources (i.e., wind, photovoltaic, biogas, waterpower, etc.), will compel economies in some regions to undergo fundamental structural changes. As the German government decided in 2020 to desist from burning coal for power production by 2038 at the latest (1), the federal states where lignite mining is a major commercial sector will need to establish new commercial sectors, as many jobs in these regions depend on that industry. Over the last 20 years, a number of projects focused on Power-to-X technology development have been undertaken in Europe (2). In the Rhenish coal district for instance – the region between Cologne, Aachen, and Düsseldorf – the Federal Ministry of Education and Research (BMBF) is currently promoting the development of new Power-to-X value chains for sustainable energy production and utilization. The ‘X’ could stand for synthetic gases, fuels or chemicals, and the goal of these technologies is to either store surplus of renewable electrical energy in the form of

chemical energy carriers, or produce valuable products for the chemical industry or transportation sector. Power-to-Syngas or Power-to-CO are two possible value chains, wherein electrical energy and CO_2 from the atmosphere or industrial point sources can be transferred to syngas ($CO + H_2$) or carbon monoxide (CO), both important intermediates in the chemical industry or for the production of synthetic fuels. For both of these value chains, SOC technology is an optimal vehicle due to the high faradaic efficiency and reversibility of cells due to their high operating temperatures. However, solid oxide electrolysis cell (SOEC) technology for CO_2 electrolysis is not yet highly commercialized on a large industrial scale, like polymer electrolyte membrane (PEM) or alkaline electrolysis cell technologies, but it is definitely ready for scale-up and has already entered the market in small, pilot-scale plants (3-5).

However, the remarkably high performance and long-term stability of conventional SOCs, especially in CO_2 electrolysis operation, has not yet been demonstrated. The aim of this work is to rectify this and present some more detailed insights into the electrochemical processes within the electrodes and to perform CO_2 electrolysis experiments on the cells in one of our SOC stacks for the first time. The migration of nickel in the fuel electrode is one of the main reasons for the degradation of SOCs in long-term steam electrolysis operation (6). The resulting change in the electrode's microstructure induces a distinct increase in the serial resistance of the cells, as electric contacting through the Ni grains is lost to some extent. In addition, carbon deposition and sulfur poisoning are known to appear in the fuel electrode of conventional SOCs with Ni/YSZ electrodes under specific conditions of CO_2 electrolysis operation (7). It is likely that the fuel electrodes of commonly used SOCs are not yet suitable for reliable operation in CO_2 electrolysis applications. Modifications of the microstructure and new electrode materials appear to be inevitable in order to guarantee a good efficiency and long-term stability of cells under these conditions.

Experimental

Solid Oxide Cells and Stack Components

For the electrolysis experiments presented in this study, conventional planar anode-supported cells (ASCs; fuel electrode = anode in fuel cell mode) were used (8). Commercial cell manufacturer CeramTec (Marktredwitz, Germany) purchased the half-cells, and a diffusion barrier and air electrode layer were added in the laboratory. These cells consisted of a porous support backbone (~300 µm) made of a Ni(O)/8YSZ cermet by means of tape casting, followed by a functional layer of fuel electrode material from the same material, but with a finer microstructure, a dense ceramic electrolyte layer of about 10 µm thickness made of 8YSZ, a diffusion barrier layer from a screen-printed GDC and, finally, a screen printed LSCF air electrode (Figure 1a). The cells, with dimensions of 100 x 100 mm^2, were tested in JÜLICH F10 short-stacks, which is a robust stack design utilized for R&D applications (Figure 1b). The contacting of the cells with the frames and interconnects within the stack was conducted by either Ni-mesh on the fuel electrode side, or by a coarse LSCF contact layer applied by screen printing on top of the air electrode. Sealing of the cells within the metallic frames and interconnects (Crofer22APU) was performed using an in-house-developed glass sealant and planar mica gaskets that assured the sealing of the stack to the test bench.

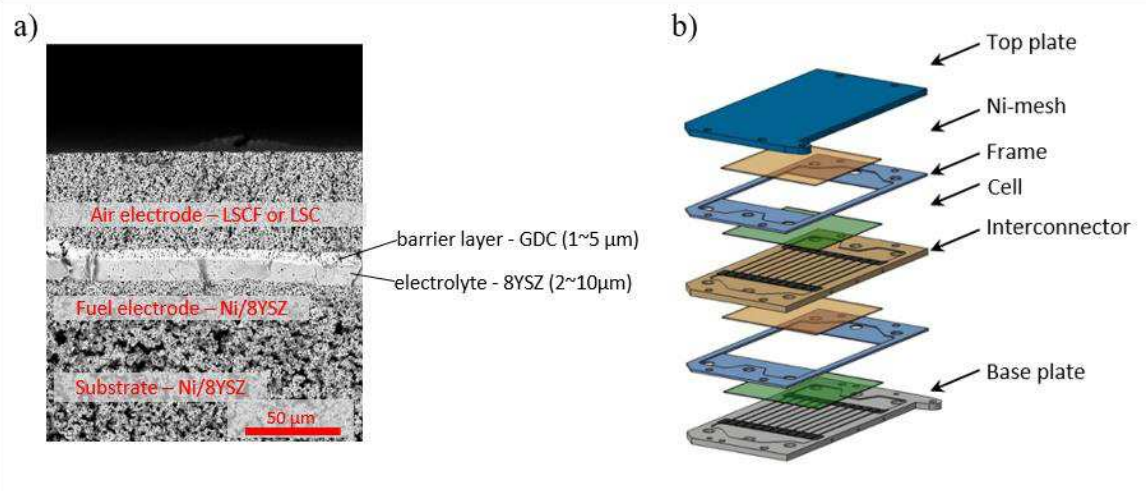

Figure 1. a) Cross-section of a typical anode-supported solid oxide cell; b) components of an F10 short-stack as the base- and top-plate, metallic interconnects, with a Ni-mesh for contacting the substrate of the cell to the interconnects, and the cells fitting inside the metallic frames; Reproduced with permission (9), Copyright Elsevier (2015).

In this study, we tested stacks with four or five cell layers of 80 cm^2 active cell area each (the air electrode limited the maximum cell area), which were connected within the stack in series. The cell voltages were measured separately for each layer using platinum wires, which were welded to the interconnectors above and below the cell, with the power electronics connected to the current collectors at the top- and base-plate of the stack.

Short-Stack Tests on the SOC Test Bench

The stack tests reported in this paper were performed on a furnace-hooded test bench on which the stack was hydraulically braced to the mounting plate (Figure 2). Gas mixing and evaporation units provided the required gas supply, and the exhaust gas was cooled by water circulation prior to leaving the test bench. The setup was also equipped with the necessary power electronics for determining the current-voltage characteristics (electronic load for fuel cell and power supply for electrolysis) and a mobile impedance analyzer (a Zahner Zennium X workstation equipped with a PP211 and EL-1000).

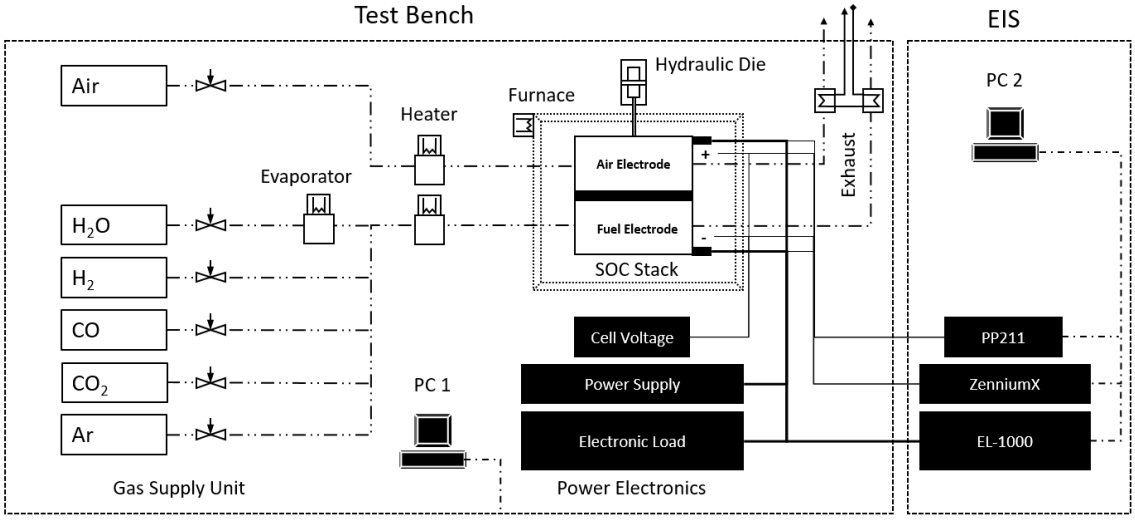

Figure 2. Schematic setup of the SOC test bench and connection of the EIS equipment.

Before the stack-tests could be conducted, some essential modifications on the test bench had to be implemented in order to ensure safe and reliable operation in CO_2 electrolysis mode. It is known from thermodynamics that, in accordance with the *Boudouard equilibrium* (Eq. 1), solid carbon black (soot) can be formed within a gas stream at high concentrations of carbon monoxide (CO). The critical CO concentration and temperature, according to carbon activity α, was calculated by using a self-programmed equilibrium solver in Matlab:

$$2\ CO \leftrightarrow CO_2 + \mathbf{C_{(s)}} \qquad [1]$$

As a rule of thumb, it can be assumed that with a higher amount of CO in the gas mixture and at lower temperatures, the carbon activity α becomes larger and more soot formation is to be expected within the stack and/or the exhaust tubes of the test bench. When α becomes larger than 1, soot can be thermodynamically formed. The amount of CO in the exhaust gas increases with the current density during stack operation in CO_2 electrolysis mode, as with a higher conversion rate, more CO_2 is electrochemically reduced to CO. In a worst-case scenario, soot that is leaving the stack could block the exhaust line and lead to severe damage of the stack or the entire test bench. Within the porosity of the fuel electrode, soot is also suspected of blocking the triple-phase boundaries and consequently significantly reducing the electrochemical performance of the solid oxide cell.

Finally, a possible solution for avoiding soot in the exhaust line was identified by adding steam (H_2O) to the exhaust gas emanating from the stack, whereby the thermodynamic equilibrium shifted away from CO to CO_2 in the *water-gas shift reaction* (Eq. 2). Therefore, the formation of soot in the exhaust gas is reliably prohibited, even at decreasing temperatures. This method was patented by Sunfire GmbH (Dresden, Germany) (10). At temperatures below 300 °C, soot formation should not be feared, as the reaction kinetics for the *Boudouard reaction* are too slow:

$$CO + \mathbf{H_2O} \leftrightarrow CO_2 + H_2 \qquad [2]$$

Measurement of Cell Performance during Electrolysis Operation

The performance of SOCs is typically determined by recording the current-voltage characteristics (IV-curves), where the cell voltage is monitored as a function of the current (or current density). Therefore, a positive current (electric load) is applied to the cell or stack for fuel cell operation (SOFC) and a negative current (electric power) for electrolysis operation (SOEC). In this study, the IV-curves were performed at increasing (or decreasing) current ramps of 20 A/min and the cell voltage was measured every 15 seconds after each step of 5 A, respectively. The IV-curves were recorded at different stack temperatures and varying fuel gas compositions in order to obtain a broad overview of the limiting factors for cell performance. Accompanying the IV-curves, the electrochemical impedance spectra were recorded as well, as described in the following section.

For this study, we measured the cell performance in three different operating modes, namely pure **steam electrolysis**, **co-electrolysis**, and **dry CO_2 electrolysis**. The following scheme (Figure 3) illustrates the electrochemical processes in these different modes. In co-electrolysis mode, CO_2 is mostly not electrochemically converted into CO, but by reacting with H_2 from the exhaust in the *reverse water-gas shift* reaction (RWGS).

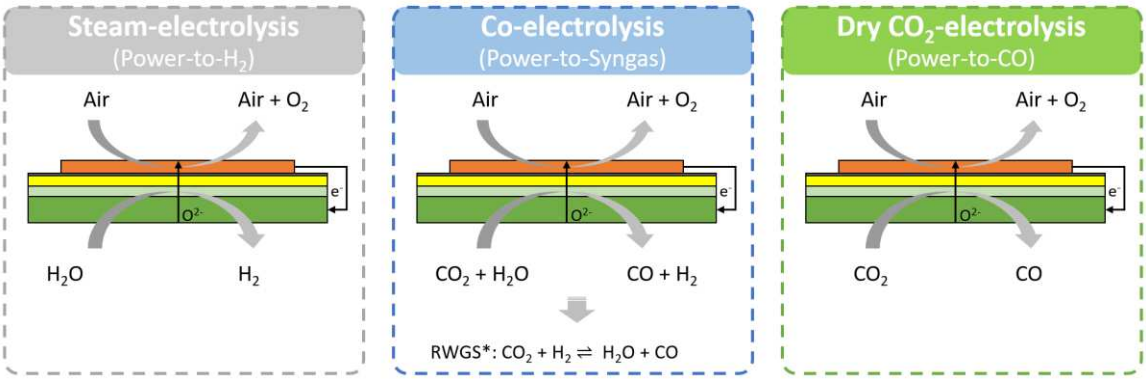

Figure 3. Gas conversion reactions in three different electrolysis modes.

Electrochemical Impedance Spectroscopy and the Distribution of Relaxation Times (DRT)

Electrochemical impedance spectroscopy (EIS) is a commonly used analytical tool that enables more detailed insights into electrochemical processes within SOCs to be obtained, especially at the interfaces and triple-phase boundaries of the electrodes. As the measurements were being taken, a small alternating current was applied to the entire stack while the impedance response of each cell was measured separately using the impedance analyzer. For our measurements, we selected an alternating current of ±2 A to a direct current of -5 A (for electrolysis operation) during the EIS measurement. A frequency range between 50 kHz and 100 mHz was measured with 15/30 steps per decade and 20/40 measurement periods (at lower limit/above 66 Hz). The impedance spectra were analyzed by plotting the Nyquist plot and calculating the distribution of the relaxation times (DRT). For the DRT analysis, we used the freely available Matlab toolbox, "DRTtools" (11). We also employed a *Gaussian* method of discretization with *combined Re-Im Data*, a regularization parameter of *1 E-4* and *Fitting with Inductance*. For the radial bias function, we used a regularization derivative of the *second order* and, for the shape control, a *Coefficient to FWHM* factor of *0.5*. In order to quantify the DRT results concerning the share of different polarization processes to the total cell resistance, we measured the area under the DRT peaks and calculated the resistance values from that data. Therefore, we plotted $\gamma(\tau)$ versus $ln(\tau)$ and integrated the area below each single peak using *Origin Lab* and multiplied the results with the corresponding active cell area of 80 cm^2. The results were then evaluated and reflect the individual contributions of the different electrode processes to the cell resistance.

Results

Cell Performance in Different Electrolysis Operation Modes

The electrochemical performance of the SOCs was determined for different electrolysis modes, as described in the experimental section above. In pure steam electrolysis mode, H_2O was reduced within the fuel electrode to produce hydrogen (H_2). When also adding CO_2 together with H_2O to the fuel electrode of the cells, both could be simultaneously converted into CO and H_2 in co-electrolysis mode. In this case, the RWGS reaction helped in the production of more CO from CO_2. In dry CO_2 electrolysis mode, only CO_2 (together

with some quantity of CO as the reducing agent) was added to the fuel electrode, and the CO_2 then had to be converted into CO by the electrochemical reaction alone.

In an initial attempt, the current-voltage characteristics and electrochemical impedance were measured in three different gas compositions, one for each of the described electrolysis modes at 800 °C. For steam electrolysis mode, a mixture of 1:1 (H_2O:H_2), for co-electrolysis mode, a mixture of 1:1:1 (H_2O:CO_2:H_2), and for CO_2 electrolysis mode a mixture of 1:1 (CO_2:CO) was set and the IV-curves and impedance spectra were recorded in fuel cell (SOFC) and electrolysis (SOEC) operation modes, as described above.

TABLE I. Gas composition of the different electrolysis modes; slm: standard liters per minute (0 °C, 1 atm).

Electrolysis mode	H_2O [slm]	H_2 [slm]	CO_2 [slm]	CO [slm]
Steam electrolysis	5.58	5.58	-	-
Co-electrolysis	5.58	5.58	5.58	-
CO_2 electrolysis	-	-	5.58	5.58

The following graph shows the IV-curves of the three different gas compositions as listed in TABLE I for an F10 stack with five cells included, but for reasons of clarity, only the mean cell voltage is illustrated here (Figure 4). It is clearly visible from the data that there is no clear difference in cell performance between the gas composition for steam electrolysis and co-electrolysis. Only the open cell voltage was slightly lower for co-electrolysis mode, which directly relates to the lower Nernst potential when additional CO_2 is present in the gas mixture. Apart from that, the IV-curve follows the trend of that from pure steam electrolysis in both fuel cell and electrolysis modes.

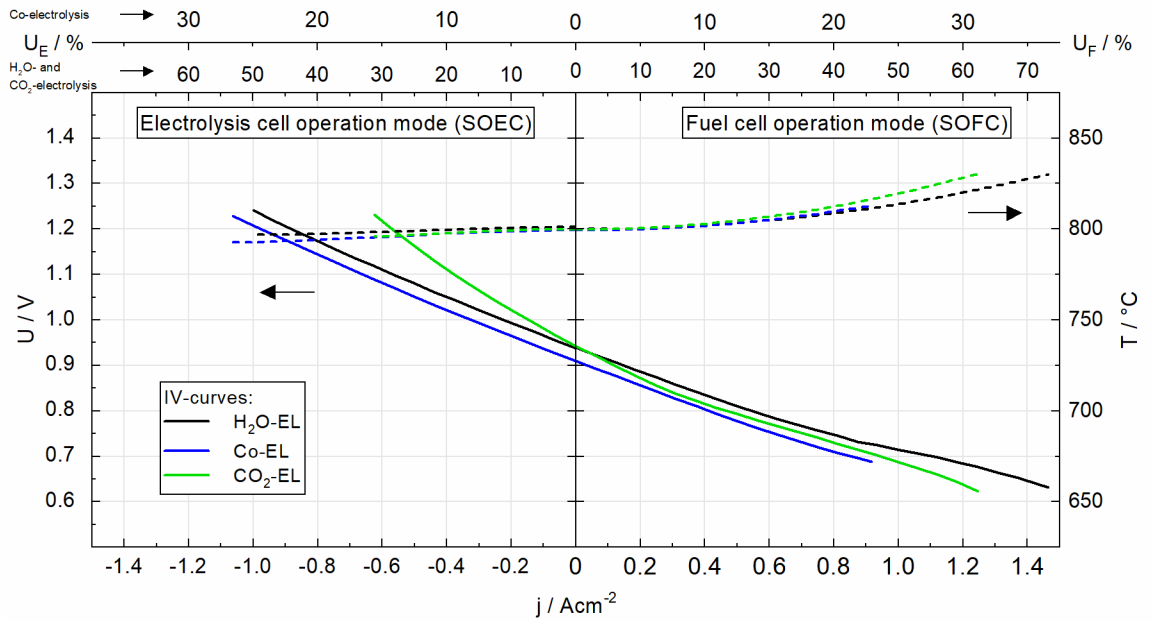

Figure 4. Current-voltage characteristics of solid oxide cells in different electrolysis operation modes at 800 °C. Note the different fuel utilization and conversion rates in co-electrolysis mode.

During the IV-curves in electrolysis operation (U_E), the conversion rate reached about 50% for steam electrolysis, 25% for the co-electrolysis mixture, and approximately 30% for CO_2 electrolysis mode. In fuel cell mode, about 70% of the hydrogen in the fuel could

be utilized (U_F) for the current H_2O/H_2 mixture at a cell voltage of close to 0.6 V. In a co-electrolysis gas mixture, these high performances could not be reached, as one cell in the stack started to lose contact during the measurements and therefore voltage of this cell dropped too much, and the measurement had to be stopped prior to reaching higher current densities. CO utilization in the third gas mixture worked as well in SOFC mode with a fuel utilization of about 30% of the fed CO. Furthermore, the temperature evaluation in the stack was measured in a representative position among the IV-curves and was plotted in the graph on the right-hand axis.

Along with the IV-curves, EIS measurements were performed for each gas composition at a low current of +5 A for SOFC and -5 A for SOEC mode, with a ±2 A alternating current. Figure 5 shows the Nyquist plots and DRT resolution of one of the cells (layer 3) within the stack. The results indicate no major difference in the electrode performance between the steam- and co-electrolysis gas mixtures, except for slight variations in the frequency range between 100 and 1000 Hz. However, when we consider the gas composition for pure CO_2 electrolysis operation, the charge transfer process involved in the electrocatalytic reduction of CO_2 in the fuel electrode, visible at about 1 kHz in the DRT, was strongly decelerated compared to the reduction of H_2O. This also indicates that under the given conditions in the co-electrolysis experiment, only H_2O was electrochemically reduced, and the CO_2 was only converted by means of the RWGS reaction. Moreover, gas diffusion in the Ni/YSZ substrate was limited for dry gas compositions containing only CO_2 + CO, as can be seen from the impedance spectra in the low-frequency region between 1 and 10 Hz.

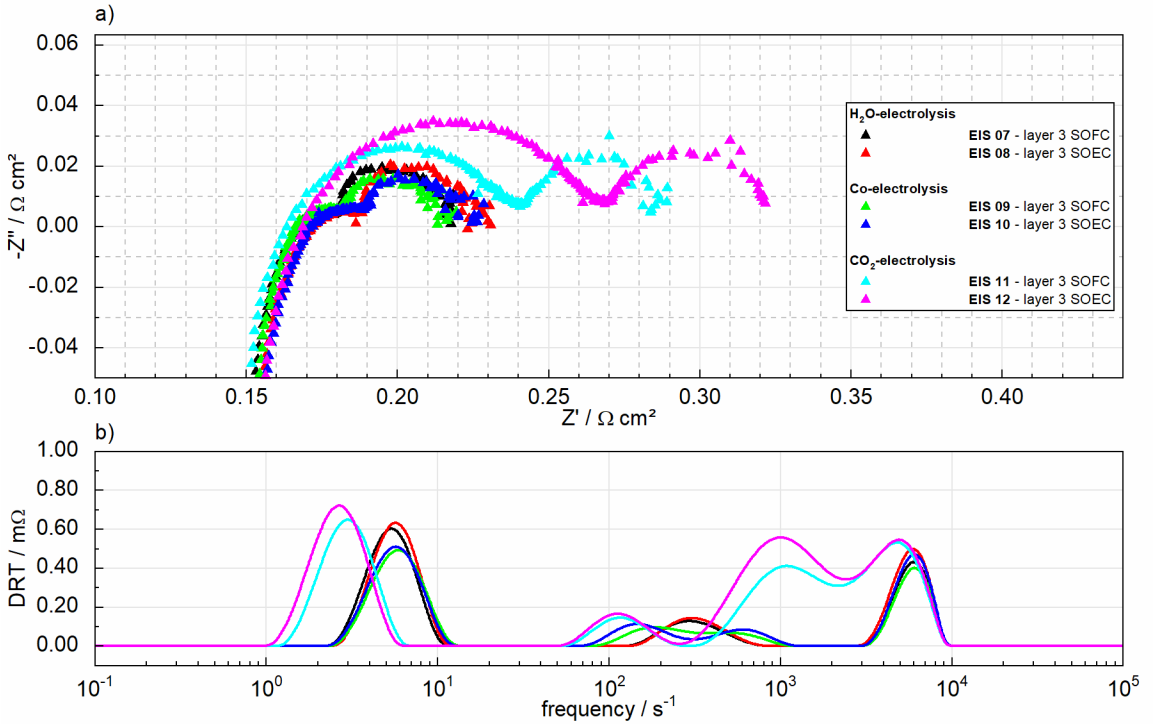

Figure 5. Electrochemical impedance data of SOCs in different electrolysis operation modes at 800 °C in fuel cell mode (SOFC) and electrolysis mode (SOEC); a) Nyquist plot with real (Z`) and imaginary (Z``) part of the impedance; and b) the DRT solution of the spectra.

Influence of the Temperature on Cell Performance during Electrolysis Operation

The influence of the operating temperature on the electrochemical performance was investigated in three different electrolysis modes at temperatures of 700–800 °C. Therefore, IV-curves and EIS measurements were performed at a second F10-stack with four layers under the conditions listed in TABLE II.

TABLE II. Operating conditions for different gas compositions at different temperatures; slm: standard liters per minute (0 °C, 1 atm).

Operation mode	T [°C]	H_2O [slm | %]	H_2 [slm | %]	CO_2 [slm | %]	CO [slm | %]
H_2O electrolysis	800	4.5 | 90	0.5 | 10	-	-
H_2O electrolysis	750	4.5 | 90	0.5 | 10	-	-
H_2O electrolysis	700	4.5 | 90	0.5 | 10	-	-
Co-electrolysis	800	3.0 | 60	0.5 | 10	1.5 | 30	-
Co-electrolysis	750	3.0 | 60	0.5 | 10	1.5 | 30	-
Co-electrolysis	700	3.0 | 60	0.5 | 10	1.5 | 30	-
CO_2 electrolysis	800	-	-	4.8 | 90	0.5 | 10
CO_2 electrolysis	750	-	-	4.8 | 90	0.5 | 10
CO_2 electrolysis	700	-	-	4.8 | 90	0.5 | 10

Figure 6 illustrates the corresponding results for the current-voltage characteristics (a), represented by the mean cell voltage of the four cells in the stack, and with impedance data that was plotted for one single cell (layer 4). The three different gas compositions were tested in the stack at temperatures of 800, 750, and 700 °C, respectively. The IV-curves and Nyquist plots of the measurement results indicate a loss in performance of the cells for all electrolysis modes with decreasing temperature. Serial (ohmic) resistance increased at lower temperatures at the same order of magnitude for all three gas compositions, as can be seen from the Nyquist plot in Figure 6 b). A major difference in the polarization resistance in the middle and high frequency ranges of the DRT (Figure 6 c)) appeared at operation temperatures below 750 °C, especially in CO_2 electrolysis mode. Here, a strong increase and broadening of the DRT peaks was observed at lower temperatures. Also, gas diffusion in the porous substrate, which is usually visible in the low-frequency peak of the DRT, appears to be inhibited in CO_2 electrolysis mode.

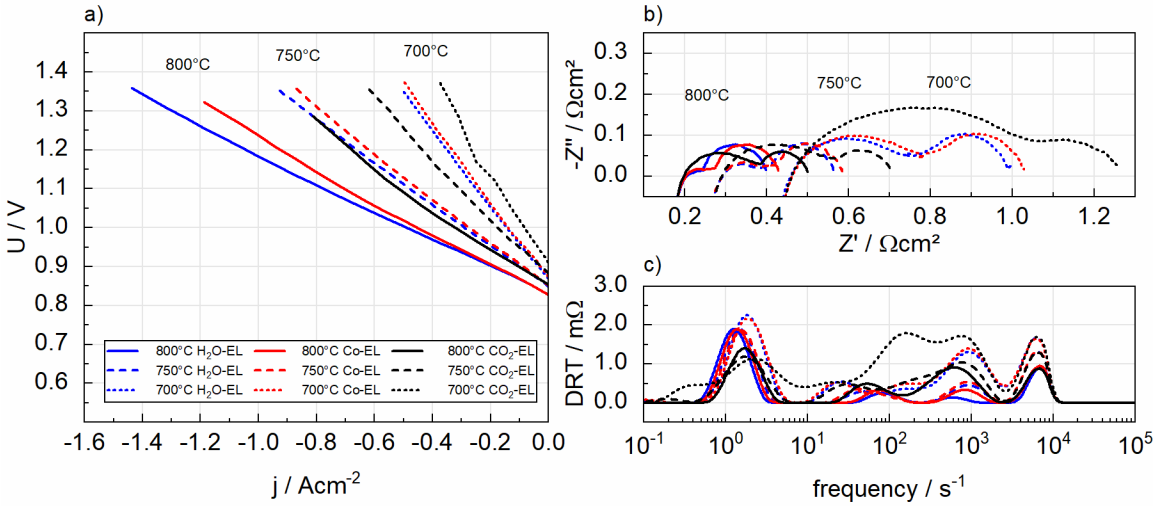

Figure 6. Electrochemical performance of solid oxide cells at different gas compositions as a function of temperature; a) IV-curves; b) Nyquist plot from the EIS; and c) the DRT resolution of the EIS data.

Influence of the CO_2:CO Ratio on CO_2 Electrolysis Performance

Variation of the CO_2:CO ratio in the pure CO_2 electrolysis mode was conducted in a measurement series with a constant total fuel flux, and the EIS measurements were performed for each composition, as listed in TABLE III. The CO_2 content in the mixture was varied from 20–90% and balanced by CO.

TABLE III. Gas compositions for the CO_2:CO ratio variation; slm: standard liters per minute (0 °C, 1 atm); the conversion rate was calculated at a DC current of -5 A, which was applied to the stack during the EIS measurement; the total flux of the fuel was kept constant.

CO_2 : CO	**CO_2 [slm]**	**CO [slm]**	**Total [slm]**	**CO_2 conversion @ -5 A [%]**
20 : 80 (0.25 : 1)	2.23	8.92	11.15	7.81
30 : 70 (0.43 : 1)	3.35	7.81	11.15	5.21
40 : 60 (0.67 : 1)	4.46	6.69	11.15	3.91
50 : 50 (1 : 1)	5.58	5.58	11.15	3.13
60 : 40 (1.5 : 1)	6.69	4.46	11.15	2.60
70 : 30 (2.33 : 1)	7.81	3.35	11.15	2.23
80 : 20 (4 : 1)	8.92	2.23	11.15	1.95
90 : 10 (9 : 1)	10.04	1.12	11.15	1.74

The low-frequency processes – including the gas diffusion in the porous Ni/YSZ substrate of the cells and gas conversion – were influenced most strongly, as is shown in Figure 7, in the low-frequency part of the spectra (the second semicircle on the right-hand side of the Nyquist plot and, accordingly, the first peak in the DRT plot). As the CO_2 content increases from the dark to brighter colors in Figure 7, the polarization resistance in the fuel electrode decreases (most likely the charge transfer process, P3). The frequency ranges of the calculated DRT peaks and their common attribution to the corresponding electrochemical processes in SOCs are listed in TABLE IV and labeled in Figure 7 b with the letters P1–P4. The serial resistance (R_Ω) and P4 in the DRT plot were almost not influenced by the gas composition, which both primarily depend on the ionic transport rate, either in the solid electrolyte or in the ceramic particles of the fuel electrode. The ionic conductivity in the O^{2-}-conducting 8YSZ material is mainly activated by the temperature, and therefore we do not observe any deviation, as the measurements were all performed at the same temperature of 800 °C.

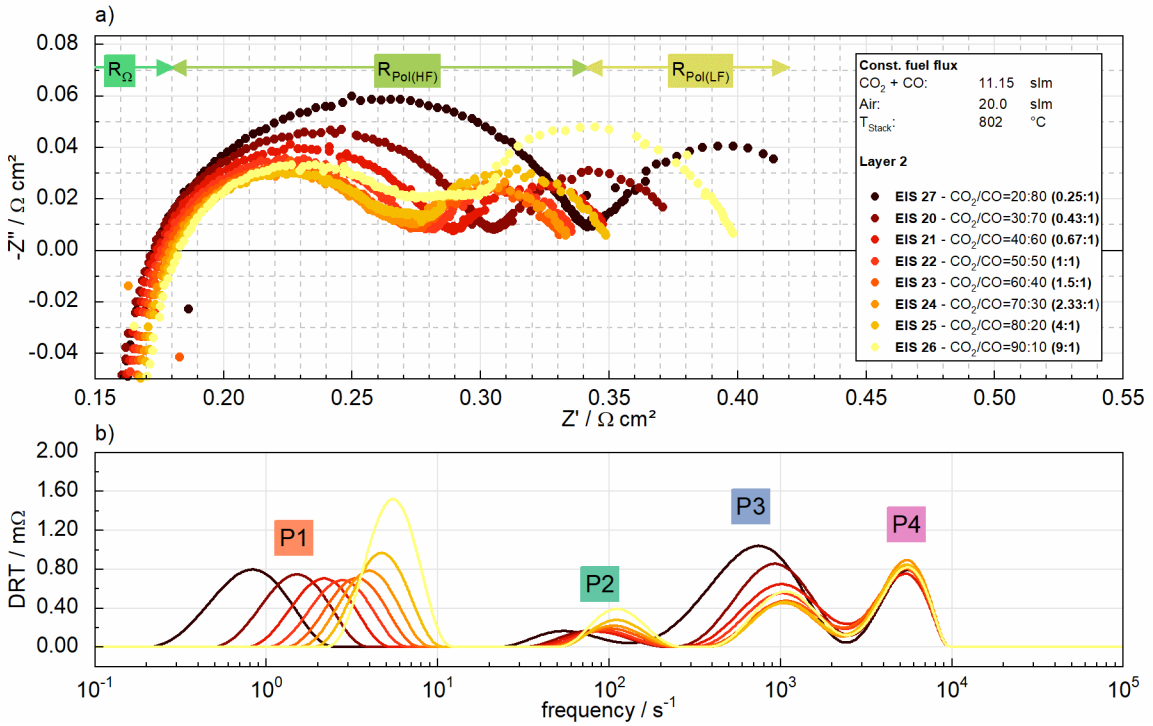

Figure 7. Electrochemical impedance of one cell in the stack measured at different CO_2:CO ratios in the fuel at 800 °C; the total gas flux was kept constant; a) Nyquist plot; and b) the DRT.

In the DRT results, we did not observe any influence on the polarization from the air electrode, as the performance of these materials is optimal at temperatures above 750 °C and the DRT peak visible at position P2 should therefore only be due to gas diffusion limitations.

TABLE IV. Typical attribution of the DRT peaks to (electrochemical) processes in the electrodes of SOCs.

DRT peak #	Frequency range	Dominating processes
P1	500 mHz–25 Hz	Gas diffusion in the substrate coupled with gas conversion
P2	25 Hz–250 Hz	Air electrode polarization + secondary peak for gas diffusion
P3	250 Hz–2.5 kHz	Charge transfer process in the fuel electrode
P4	2.5 kHz–10 kHz	Ionic transport in the fuel electrode

For the sake of clarity, we have plotted the different contributions to the cell resistance in two bar graphs in Figure 8. One graph is for the ohmic and polarization resistance directly read from the real part Z` of the Nyquist plots (Figure 8 a)) and one for the calculated areas under the DRT peaks, which can be translated into polarization values as well (Figure 8b). We can observe a clear indication of increased gas diffusion limitation with CO_2 contents of more than 50%, both in $R_{Pol(LF)}$ and in the area of the first DRT peak P1. The high frequency part of the impedance spectra ($R_{Pol(HF)}$) is represented by DRT peaks P2–P4 and the corresponding resistance values in Figure 8a agreed well with the sum of the values for P2, P3, and P4 in Figure 8b. As expected, the serial resistance (R_Ω) and ionic transport in the fuel electrode (P4) were not affected by the amounts of CO_2 and CO in the fuel.

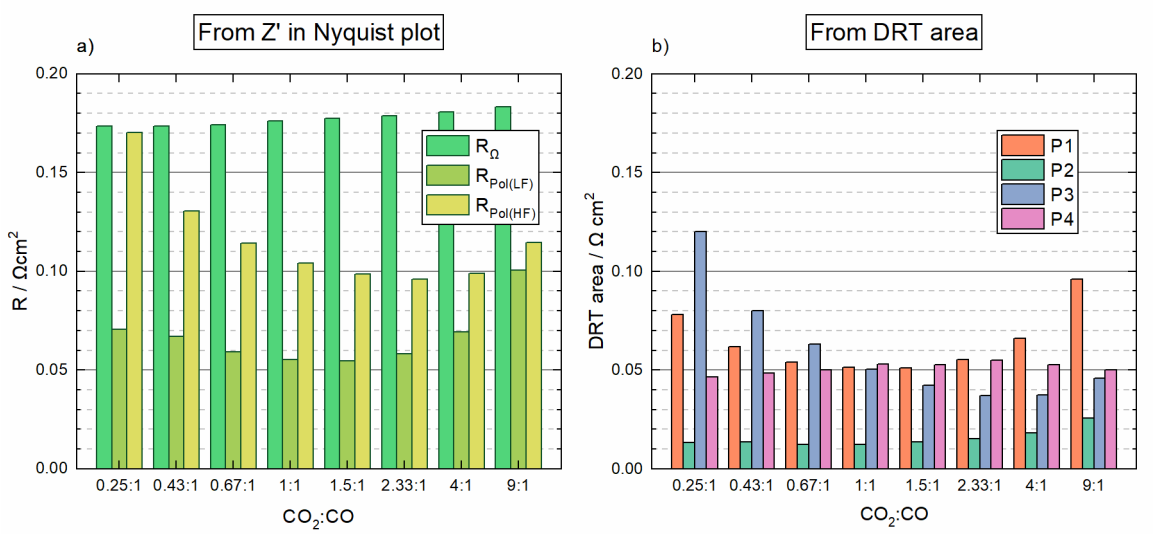

Figure 8. Resistance values for the serial and cell polarization resistance as a function of the gas composition determined from: a) the Nyquist plot in Figure 7a; and b) the peak areas of the DRT data.

Conclusions

The presented results demonstrate the general operability of the conventionally-utilized SOCs with an Ni/YSZ fuel electrode in different operation modes, including co- and CO_2-electrolysis. The electrochemical performance was acceptable for gas compositions containing steam and CO_2 for co-electrolysis operation, but worse for pure CO_2 electrolysis. Especially in SOEC mode, the cell polarization in the middle and high frequency ranges of the DRT increased drastically when switching to dry CO_2/CO mixtures. Additionally, gas diffusion polarization was significantly enlarged in pure CO_2 electrolysis operation.

The serial and polarization resistances of the cells increased with decreasing temperature for all operating modes, but at the largest extent, in the dry CO_2/CO mixtures. The results from the EIS analysis indicated a general problem in the charge transfer process for pure CO_2 electrolysis operation within the fuel electrode, especially at temperatures below 750 °C. For this reason, we conclude that the materials and microstructures of the fuel electrode in our actual cells are not yet optimized for CO_2 electrolysis operation. New material combinations, such as a cermet made of nickel and gadolinium-doped ceria (GDC) and a coarsening of the microstructure of the fuel electrode and the support could help to improve the electrochemical performance.

Carbon deposition and Ni migration could not be observed, as the stack was not opened, and the cells were not analyzed following operation. Moreover, the operation times of the stacks in electrolysis mode containing CO_2 in the fuel were very limited until now, and therefore no strong degradation of the cells was expected. However, the performance of the cells decreased following operation with a high conversion rate in CO_2 electrolysis mode, which could offer a hint about potential carbon deposition within the fuel electrodes.

Variation in the CO_2:CO ratio in the fuel supply indicated a gas diffusion limitation in the porous cell substrate at higher contents of CO_2, which reduces the electrochemical performance at higher conversion rates. On the other hand, the charge transfer process in the fuel electrode was more favorable with increasing portions of CO_2 in the fuel. The ionic conductivity of the electrolyte and the fuel electrode material remained unaffected by the

fuel composition at a constant operating temperature. At a temperature of 800 °C – where the series of the CO_2/CO variation was conducted – no information about the performance of the air electrode was visible in the EIS data, as these usually appear at lower temperatures or at varying oxygen partial pressure gradients across the cell.

In further stack tests, more investigations regarding the electrochemical performance of the cells in CO_2 electrolysis mode are planned. Impedance analyses of a stack under current could provide more information about the performance, such as the area-specific resistance (ASR) of the cells. By operating the stacks at lower temperatures, one may learn more about the contribution of the air electrode to the total cell resistance. Finally, long-term operation over several thousand hours in CO_2 electrolysis mode with and without contaminations would be necessary to identify and understand potential degradation effects such as Ni-migration, carbon deposition or sulfur poisoning within SOCs. It is assumed that the development of new cell types with Ni/GDC fuel electrodes could significantly increase the performance and durability of the cells, which is to be confirmed in future cell and stack tests.

Acknowledgments

The authors acknowledge the financial support of the Federal Ministry of Education and Research (BMBF) under the project iNEW (03SF0589A). Furthermore, the contributions of all colleagues working on the SOC project at the Forschungszentrum Jülich are gratefully acknowledged. Many thanks as well to Mr. Christopher Wood for thoroughly proofreading the manuscript.

References

1. http://dipbt.bundestag.de/extrakt/ba/WP19/2587/258735.html; Access 2021-04-27.
2. C. Wulf, P. Zapp and A. Schreiber, *Front. Energy Res.*, 8(191), 2020.
3. A. Hauch, R. Küngas, P. Blennow, A.B. Hansen, J.B. Hansen, B.V. Mathiesen and M.B. Morgensen, *Science*, 370(6513), eaba6118 (2020).
4. R. Küngas, P. Blennow, T. Heiredal-Clausen, T. Holt Nørby, J. Rass-Hansen, J.B. Hansen and P.G. Moses, *ECS Trans.*, 91(1), 215-23 (2019).
5. C. Geipel,K. Hauptmeier, K. Herbrig, F. Mittmann, M. Münch, M. Pötschke, L. Reichel, T. Strohbach, T. Seidel, A. Surrey and C. Walter, *ECS Trans.*, 91(1), 123-32 (2019).
6. X. Sun, P.V. Hendriksen, M.B. Mogensen and M. Chen, *Fuel Cells*, 19(6), p. 740-7 (2019).
7. T. L. Skafte, P. Blennow, J. Hjelm, and C. Graves, *J. Power Sources*, 373(0), p. 54-60 (2018).
8. L. Blum, L.G.J. de Haart, J. Malzbender, N.H. Menzler, J. Remmel and R. Steinberger-Wilckens, *J. Power Sources*, 241(0), p. 477-85 (2013).
9. Q. Fang, L. Blum, R. Peters, M. Peksen, P. Batfalsky and D. Stolten, *Int. J. Hydrog. Energy*, 40(2), p. 1128-36 (2015).
10. D. Rüger, C. Berninghausen, C. Klahn, S. Becker and R. Blumentritt R, Sunfire GmbH, 01237 Dresden (DE), *German Patent*, EP 3 415 466 A1. 2017, 19.12.2018.
11. T.H. Wan, M. Saccoccio, C. Chen and F. Ciucci, *Electrochim. Acta*, 184, p. 483 (2015).